SATELLITE-BASED CORRELATION STUDIES OF MESOSPHERIC O_2 AND OH INFRARED EMISSIONS

Brandon K. Thurgood

Rocky Mountain NASA Space Grant Consortium
Utah State University, Logan UT

ABSTRACT

The Mesosphere and Lower Thermosphere/Ionosphere (MLTI) plays an important role in the energy balance of the Earth-Sun planetary system. The SABER (Sounding of the Atmosphere using Broadband Emission Radiometry) instrument on NASAs TIMED (Thermosphere Ionosphere Mesosphere Energetics and Dynamics) satellite is a spatially scanning 10-channel infrared radiometer. To aid in the modeling of the photo-chemical dynamics that take place in the MLTI region, a series of correlations concerning three radiometric airglow bands of SABER are explored. The three bands of interest are $O_2(^1\triangle_g)$, OH(9-7;8-6) and OH(5-3), centered at wavelengths of 1.27, 2.06 and 1.64 μm, respectively. It was found that both the $O_2(^1\triangle_g)$ and OH($\triangle v = 2$) nighttime airglow volume emission rates have consistently brighter values and lower altitudes at near equatorial latitudes compared with values at mid-latitudes. Two correlations are presented herein: (1) latitudinal and (2) global. The correlations performed showed consistent results. The more reliable results come from the global correlation using a binning technique that allowed for more data. The binning technique also made it possible to view the correlations over the entire globe. The dual OH airglow bands exhibited a strong correlation (0.85 to 1.0). The O_2 1.27 μm airglow band showed a strong correlation (0.8 to 1.0) with the OH 2.06 μm airglow band. The O_2 1.27 μm airglow band is less correlated (0.6 to 0.8) with the OH 1.64 μm airglow band.

1. INTRODUCTION

The photo-chemical reactions that occur in the Mesosphere and Lower Thermosphere/Ionosphere (MLTI) region lead to excited $O_2{}^*$ and OH^* molecules. These excited molecules create the infrared airglow emissions that are discussed. Smith[1] and Mylnczak[2] give good explanations of the reactions important in the dynamic energetics of the MLTI region.

1.1. TIMED Mission

The TIMED satellite was launched on December 7, 2001 from Vandenberg Air Force Base, CA[3]. There are four sensors functioning aboard the TIMED satellite: Global Ultraviolet Imager (GUVI), Solar Extreme Ultraviolet Experiment (SEE), TIMED Doppler Interferometer (TIDI), and Sounding of the Atmosphere using Broadband Emission Radiometry (SABER). SABER, which is the source of the data for the research reported herein, measures infrared airglow utilizing a 10-channel spatial radiometer[3].

1.2. SABER Instrument

SABER was designed, fabricated, calibrated, and flown by the Space Dynamics Laboratory (SDL) of Utah State University (USU) and the NASA Langley Research Center(LaRC)[4]. Approximately every 58 seconds, a vertical limb scan is made using a rocking mirror to obtain emission altitude profiles from the Earth's surface up to an altitude of about 180 kilometers. Three-dimensional spatial data are thereby collected for each of the ten radiometer channels. Around 1400 to 1500 scans are made during an entire day.

Table 1 is a summary of the dedicated single O_2 and dual OH infrared channels of SABER that are of interest in this study[5]. The data from the satellite are transmitted from orbit to G & A Technical Software (GATS) in Hampton, Virginia where different levels of

Table 1. SABER Channels of Interest in this Study

SABER Channel Number	Chemical Species	Center Wavelength of IR Filter (μm)	Bandwidth ($\Delta\lambda$, μm)	Vibrational-Rotation Bands
8	OH (A)	2.06	0.230	OH(9-7); OH(8-6)
9	OH (B)	1.64	0.143	OH(5-3)
10	O_2	1.27	0.0260	$O_2(^1\Delta_g)$

processing are performed and the assembled TIMED database is made available to the SABER science team [6].

1.3. Objectives

The goal of this research is to investigate the nocturnal mesospheric oxygen and hydroxyl infrared airglow emissions and ascertain relevant correlations between data obtained by the SABER sensor onboard the TIMED satellite. Specifically, the objectives are:

- Map a global multiple-day mean, covering the spring equinox, of the peak volume emission rates (VER) for the O_2 1.27 μm, OH 2.06 μm, and OH 1.64 μm airglow for the years 2002 through 2005.
- Map a global multiple-day mean, covering the spring equinox, of the airglow layer peaks from altitude profiles for the O_2 1.27 μm, OH 2.06 μm, and OH 1.64 μm for the years 2002 through 2005.
- Process and display multiple-day mean correlations, covering the spring equinox, between the oxygen and hydroxyl airglow bands. These include correlations between OH 2.06 μm and OH 1.64 μm, O_2 1.27 μm and OH 2.06 μm, and O_2 1.27μm and OH 1.64μm over a span of four years.
- Process and display the correlations between the O_2 and OH airglow measurements over an entire years worth of data for each of the four years.

The study of the correlations helps to verify assumptions about the most important photo-chemical reactions included in the models of the MLTI region of the atmosphere. The correlations between the O_2 and OH airglow are important, as the O_2 1.27 μm and OH 2.06 μm emissions both ultimately result from dissociation of molecular oxygen by solar ultraviolet radiation. Correlation findings about the constituent airglow species of the Earth's atmosphere revealed by the study reported herein, concerning the radiative relaxation of the excited O_2 and OH molecules, will help the SABER science team better validate models for the dynamic photo-chemistry of the MLTI region.

2. RESULTS AND OBSERVATIONS

2.1. Global Mapping of Airglow Emission

The global image mappings as well as the correlation processing presented in this section result in a better understanding of the relevant photo-chemical reactions and energetics of the MLTI region of the Earth's atmosphere. Data being processed are restricted to the time period consisting of three hours after sunset until sunrise, due to the large amounts of data and the long lifetime of oxygen.

2.2. Peak VER at Spring Equinox

One of the goals for the SABER experiment was the production of two-dimensional global maps showing the infrared VERs from oxygen and hydroxyl constituents of the mesosphere. For this study, due to the wealth of available data, only the peak infrared VERs will be addressed. Figure 1 shows the effects of the hybrid Kriging interpolation [7], [8], and [9]. The individual points shown on the top are the actual locations of the scans according to the latitude and longitude. The one on the bottom are the actual data points that are smoothed or interpolated over the entire surface of the globe. The rest of the results shown herein used the hybrid Kriging interpolation method.

The following is a discussion and demonstration of a ten-day mean peak nightime VER centered around the spring equinox. Figure 2 shows the peak VERs for the O_2 1.27 μm nighttime airglow band. The peak VER values were found to be stronger by about a factor of five around the equatorial latitudes compared with mid-latitudes. The dual OH channels not shown show similar results to those stated for the O_2 channel.

2.3. Altitude of Peak VER at Spring Equinox

Figure 3 shows the altitudes of the peak VER's of the nighttime airglow corresponding to fig. 2. The airglow layer at the equator, which also corresponds to the stronger VER magnitudes, was consistently lower in altitude than at mid-latitudes.

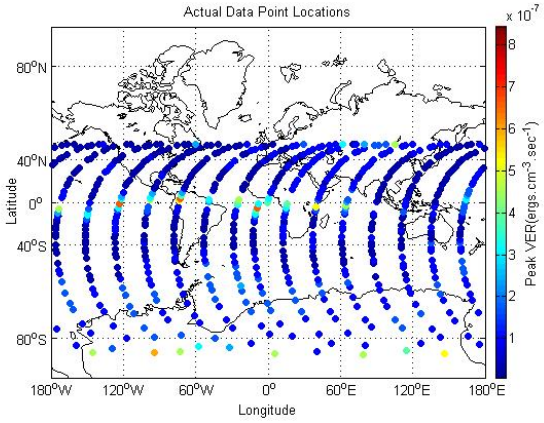

(a) Actual Data Points

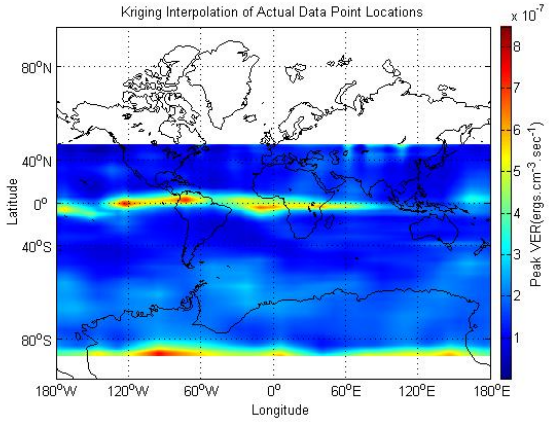

(b) Interpolation of Data Points

Fig. 1. Display of the hybrid Kriging interpolation method.

The findings are consistent with what researchers have indicated[10], namely that the airglow from O_2 infrared atmospheric airglow bands occurs at heights between 80 and 100 *km*. The dual OH bands again were consistent with the O_2 channel.

2.4. Correlation Methods

The correlation coefficient represents the linear relationship between two channels. Computation of the correlation helps the analyst to assess how variation in one channel is related to the variation in the other. The correlations described herein, as applied to the SABER data, are: (1) a latitudinal correlation and (2) a global correlation (see Thurgood [11]).

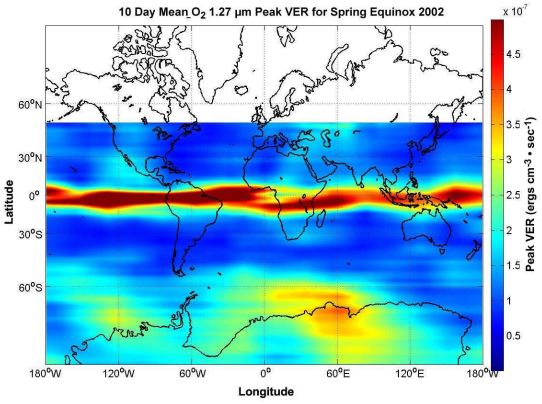

Fig. 2. Peak VER for $O_2(^1\triangle_g)$ during the spring equinox.

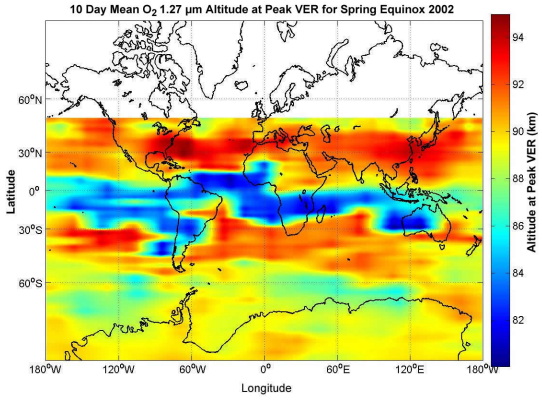

Fig. 3. Peak of the altitudinal layer for $O_2(^1\triangle_g)$ during the spring equinox.

2.5. Latitudinal Correlation

A latitudinal correlation was performed by using the airglow bands at equatorial latitudes. Each data scan that fell inside the band was parameterized as a vector. Having three parameterized vectors, corresponding to the single O_2 channel and the dual OH channels, a calculation of the cosine of the angle between any two was employed to ascertain how close the vectors resembled one another. A value of unity indicates that the angle between the vectors is zero; thus they match very well. On the other hand, a value of zero means that the vectors are perpendicular showing no correlation. Negative values indicate anti-correlation. Equations 1 through 6 mathematically model the latitudinal correlation where $\overrightarrow{U}$ and $\overrightarrow{V}$ represent any two different channels, and M and N represent the number of scans in each vector, respectively. As a data scan is observed the values for one channel are placed in vector $\overrightarrow{U}$ while the values for the other channel are placed in vector $\overrightarrow{V}$. After all values are placed in the corresponding vectors the cosine of the angle between them may be calculated.

$$\overrightarrow{U} = [U_1 ... U_M]^T \tag{1}$$

$$\overrightarrow{V} = [V_1 ... V_N]^T \tag{2}$$

$$\overrightarrow{\mathbf{1}} = [1 ... 1]^T \tag{3}$$

$$\overrightarrow{Um} = \overrightarrow{U} - \frac{\sum_{i=1}^{M} U_i}{M} \overrightarrow{\mathbf{1}} \tag{4}$$

$$\overrightarrow{Vm} = \overrightarrow{V} - \frac{\sum_{i=1}^{N} V_i}{N} \overrightarrow{\mathbf{1}} \tag{5}$$

$$\cos(\theta) = \frac{\overrightarrow{Vm}^T \overrightarrow{Um}}{\sqrt{\overrightarrow{Vm}^T \overrightarrow{Vm}} \sqrt{\overrightarrow{Um}^T \overrightarrow{Um}}} \tag{6}$$

Table 2 shows the correlation values from the four different years for the peak VERs.

Table 2. Latitudinal Peak VERs Correlations

Year	γ(OH 1.64, OH 2.06)	γ(O_2 1.27, OH 1.64)	γ(O_2 1.27, OH 2.06)
2002	0.967	0.897	0.938
2003	0.941	0.242	0.398
2004	0.859	0.632	0.788
2005	0.926	0.783	0.908

The results are as predicted. The OH 2.06 μm with OH 1.64 μm indicates strong correlation (0.85 to 0.95), the O_2 1.27 μm with OH 2.06 μm airglow indicates weak to strong correlation (0.75 to 0.95), and the O_2 1.27 μm with the OH 1.64 μm indicates the least correlated (0.64 to 0.89). To obtain more reliable correlation values that are not restricted to $\pm$ 1^o latitude, more data points are required.

2.6. Global Correlation

Latitudinal correlation previously treated showed the correlation between the airglow features. However, the correlation returned only a single mathematical value that is difficult to interpret for a global representation. The accuracy of the correlation could be suspect due to the lack of a statistically significant number of data points. The global correlation performed uses a binning technique to perform a point by point correlation that can be extended over the entire globe. This allows a correlation to be mapped over the entire Earth.

The global method is accomplished by dividing the terrestrial cartography into equal rectangular areas of latitude and longitude. If a scan lies within the rectangular area, the latitude and longitude are modified to be situated in the center of the rectangle so that a mean value may be calculated for that specific area over multiple scans. Thus, the smaller the rectangle, the closer to the actual latitude and longitude the scan will fall. For all subsequent results a rectangular region of 10^o in both the latitude and longitude was chosen. As the satellite orbits and the Earth rotates with time, a problem arises in the attempt to correlate the data over multiple days of data. The binning technique alleviates this problem making it possible to capture of all the scans over a certain area of the Earth centered at a given latitude and longitude.

Figure 4 together with Equations 7 through 18 demonstrate the process of binning the data in order to calculate a correlation[12]. Figure 4 shows the rectangle areas as if the Earth was divided into subareas. All values are initialized to zero. The designations O2, OH16, and OH20 are used to indicate the current values of O_2, OH 1.64, and OH 2.06, respectively. N is the total number of bins, subscript *k* represents the bin number, and M_k is the total number of scans per bin. Again a value close to unity for each bin indicates strong correlation, whereas a negative sign indicates anti-correlation.

$$mO2_k = \frac{\sum_{i=1}^{M_k} O2_{k,i}}{M_k} \qquad k = 1, 2, ..., N \tag{7}$$

$$mOH16_k = \frac{\sum_{i=1}^{M_k} OH16_{k,i}}{M_k} \qquad i = 1, 2, ..., M_k \tag{8}$$

$$mOH20_k = \frac{\sum_{i=1}^{M_k} OH20_{k,i}}{M_k} \tag{9}$$

$$a_k = a_k + (O2_{k,i} - mO2_k)(O2_{k,i} - mO2_k) \tag{10}$$

$$b_k = b_k + (OH16_{k,i} - mOH16_k)(OH16_{k,i} - mOH16_k) \tag{11}$$

$$c_k = c_k + (OH20_{k,i} - mOH20_k)(OH20_{k,i} - mOH20_k) \tag{12}$$

$$d_k = d_k + (OH20_{k,i} - mOH20_k)(O2_{k,i} - mO2_k) \tag{13}$$

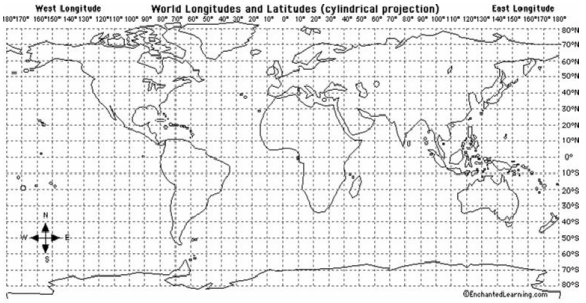

Fig. 4. Layout of the individual binning areas.

$$e_k = e_k + (O2_{k,i} - mO2_k)(OH16_{k,i} - mOH16_k) \quad (14)$$

$$f_k = f_k + (OH20_{k,i} - mOH20_k)(OH16 - mOH16_k) \quad (15)$$

$$OH20xOH16_k = \frac{f_k}{\sqrt{c_k b_k}} \quad (16)$$

$$OH20xO2_k = \frac{d_k}{\sqrt{c_k a_k}} \quad (17)$$

$$O2xOH16_k = \frac{e_k}{\sqrt{a_k b_k}} \quad (18)$$

Since a correlation number between ± 1 has been assigned to each bin, a mapping may be performed using the hybrid Kriging interpolation and a Mercator projection [7], [8], and [9]. The correlations made it possible for an entire year's worth of data to be correlated. The mapping of the correlation has led to some interesting findings that will now be discussed.

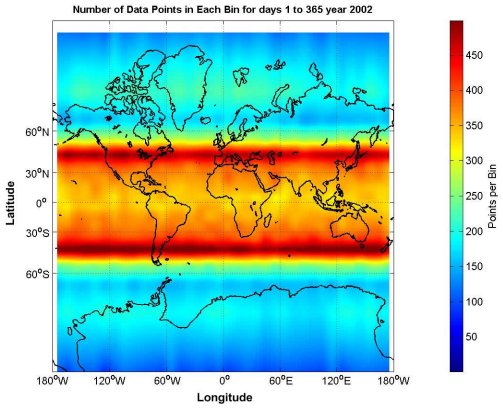

Fig. 5. The number of data points per bin over the year 2002.

Figure 5 displays the number of data points contained in each bin. A band between 45^{o}N and 55^{o}N contains more data points than any other region of the terrestrial map. Detailed investigation into the satellite orbit over the entire year was required to understand the observational results (see fig. 6. The TIMED satellite carrying SABER was injected into Earth orbit at an inclination of 74.1^o relative to the equator at a nominal altitude of 625 km. SABER looks out to the side of the spacecraft, 90^o to the direction of motion of the spacecraft. The result is that at any time the instrument can see only from about 51^o on one hemisphere to 82^o on the other hemisphere. Furthermore, every 60 days, the TIMED satellite is commanded to perform a "yaw maneuver" in which it is reoriented 180^o. Therefore, for 60 days, SABER will see from 51^o N to 82^o S, and then for the next 60 days, it sees from 51^o S to 82^o N and so on[13].

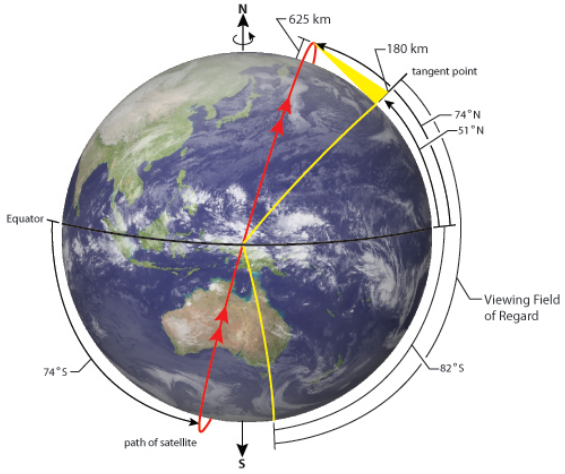

Fig. 6. The orbital and viewing fields of SABER.

The correlation of the peak VERs between the OH 2.06 μm and the O_2 1.27 μm is illustrated in fig. 7. The two OH channels are very well correlated (0.85 to 0.95). The correlation O_2 1.27 μm with OH 2.06 μm has a strong correlation (0.8 to 0.95). The O_2 1.27 μm with OH 1.64 μm shows a weak correlation (0.4 to 0.5). As the latitude increases both to the north and south the correlation decreases.

3. CONCLUSIONS

3.1. Conclusion

Because of the success of SABER and the other instruments onboard the NASA TIMED satellite, the mission has been extended beyond its originally planned

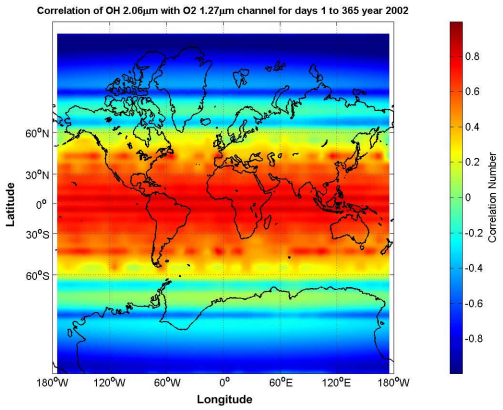

Fig. 7. Correlation of peak VER for OH 2.06 μm and O2 1.27 μm for the year 2002.

two-year life span. Four years of exceptionally good, well-calibrated data were available for this study. Due to the enormous amounts of data available this study was limited to the nighttime infrared airglow, consisting of three hours after sunset until sunrise. Algorithms were used to globally display $O_2(^1\triangle_g)$ and the OH($\triangle v = 2$) emissions at different wavelength bands from the SABER sensor. With the ability to map the peak infrared nighttime volume emission rates (VER) of the mesospheric airglow, it was observed that the $O_2(^1\triangle_g)$ and the OH($\triangle v = 2$) emission bands have consistently higher VERs near the equator than at a mid-latitudinal ranges. Furthermore, the VER peak occurs at a lower altitude over the equator than at the mid-latitudes. This latitudinal dependence was more pronounced at the solar equinoxes than at the solstices.

With the satellite orbiting at an inclination of 74^o from the equatorial plane and the rotation of the Earth underneath, most of the scans seen by SABER are within $\pm$ 50^o in latitude. Measurements are made over the latitude ranging from 51^oS to 82^oN with alternating hemispheric coverage every 60 days.

Three different types of correlations of the Atmospheric Infrared $O_2(^1\triangle_g)$ and the OH($\triangle v = 2$) Meinel nighttime airglow were made. First, a latitudinal correlation was performed by using the airglow bands at equatorial latitudes. A parameterized curve was created from all the data points falling inside $\pm 1^o$ in latitude. The cosine of the angle between two different airglow bands was then calculated to describe the correlation of the two bands. The closer the value is to unity the higher the correlation. A zero signifies no correlation and a negative unity indicates anti-correlation. Second, a normalized minimum squared error (MSE) was used for the same equatorial bands as the latitudinal correlations. Lower values of MSE relate to reduced differences and consequently higher correlation between the two airglow bands. Finally, a point by point correlation was performed over the entire terrestrial sphere. The global correlation method employed a division of the global area into equal latitudinal and longitudinal rectangles. Using the rectangles as a method of binning along with the auto and cross-correlations, global correlations were performed over the terrestrial sphere. The global correlation proved to be the best method of correlation. The improved results are due to better statistics such as the ability to incorporate an entire year's worth of data and the ability to see the correlations over the entire globe.

According to the global correlation (0.9 and 1.0) the two OH airglow channels exhibited strong correlation. The global correlation for O_2 1.27 μ with the OH 2.06 μm also exhibited strong correlation (0.8 to 1.0). The O_2 1.27 μm with the OH 1.64 μm show weak correlation with a smaller global correlation (0.6 to 0.8). The three different types of correlations facilitated the processing and display of multiple-day mean correlations between the three different calibrated (level 2) nighttime infrared airglow bands measured by the SABER multi-channel radiometer in orbit on the TIMED satellite.

3.2. Future Work

Thanks to the support from the NASA Langley Research Center and the NASA Space Grant Consortium continued studies can proceed using the wealth of SABER data. The study included here was based upon the single O_2 airglow channel and the dual OH airglow channels during the nocturnal hours only. Further work on the daytime and twilight airglow is needed. Such studies could include processing correlations between the nighttime and daytime airglow emissions. Investigations into the diurnal, seasonal and solar cycle trends in global VER distributions should be made

SABER also includes other airglow emissions besides the single O_2 and the dual OH channels that should be considered as they relate to the OH Meinel and molecular oxygen atmospheric infrared vibration-rotation band emissions. Also, correlation studies could be performed with other data (such as the solar UV flux)

from the other three sensors onboard TIMED in addition to SABER.

A study of the polar regions should be explored. The correlations discussed herein have shown differing effects at higher latitudes. This could be caused by the long periods without illumination or periods with very low illumination.

As SABER continues to be operational aboard the TIMED satellite into a fifth year correlations between sunspot numbers, solar flux values, and the infrared VERs could be explored. It would be interesting to see the effect on the mesospheric O_2 and OH airglow emissions from solar effects such as solar storms.

4. ACKNOWLEDGMENTS

I would like to thank Doran Baker and the Rocky Mountain NASA Space Grant who has provided valuable guidance and support throughout this project. My gratitude extends to Dr. Marty Mlynczak of the NASA Langley Research Center and Dr. James Russell of Hampton University for their insights and responses to my inquires. To the students who spent countless hours working on the SABER project with me namely: Ricky Fielding, Kenny Reese, and Willie Harrison. A special thanks to my mother and father, Dr. and Mrs. Ronald Thurgood, not only for their financial support but for the way in which they raised me. Last but not least thanks to my incredible wife, Taneill, and my two darling little girls, Emma and Taylee, for their constant support and encouragement. I am truly blessed to have such wonderful people who have helped in so many ways.

5. REFERENCES

[1] A. K. Smith, "Physics and chemistry of the mesopause region," *Atmospheric and Solar-Terrestrial Physics*, vol. 66, pp. 839–857, 2004.

[2] M. G. Mlynczak, "A new perspective on the molecular oxygen and hydroxyl airglow emissions,," *Geophysical Research*, vol. 104, pp. 27, 535–27, 543, Nov. 1999.

[3] TIMED, A Mission to Explore One of the Last Frontiers in Earth's Atmosphere NASA TIMED Website available at http://www.timed.jhuapl.edu/WWW/.

[4] SABER Website. SABER Science Data Processing. Available at: http://saber.larc.nasa.gov.

[5] S. Hansen, J. Peterson, R. Esplin, and J. Tansock, "Component level prediction versus system level measurement of saber relative spectral response," *Remote Sensing*, vol. 24, no. 2, pp. 389–402, 2003.

[6] G. A. T. Software, "Level 2a software development document for saber," *GATS, Hampton, VA, GATS Doc No: SABER-L1BSDD-98-1.V1*.

[7] D. Krige, "A statistical approach to some basic mine valuation problems on the witwatersrand," *Chemical, Metalurgical, & Mining Society of South Africa*, vol. 52, p. 121, Dec. 1951.

[8] K. Reese, "Processing and visualization of mesospheric hydroxyl infrared emission data from the saber sensor," M.S. Thesis, Utah State University, 2005.

[9] R. Fielding, "Satellite-based investigation of mesospheric infrared emissions," M.S. Thesis, Utah State University, 2005.

[10] U. R. Embry, *A Study of O2 Infrared Radiation in the Twilight Airglow*. Phd dissertation, Utah State Univeristy, 1978.

[11] B. K. Thurgood, "Satellite-based correlation studies of mesospheric O_2 and OH infrared emissions," M.S. Thesis, Utah State University, 2006.

[12] Enchanted learning website Available at: EnchantedLearning.com.

[13] J. M. Russell, M. G. Mlynczak, L. L. Gordley, C. J. Mertens, R. Picard, M. Lopez-Puertas, D. E. Siskind, D. Baker, J. Ulwick, E. E. Remsberg, J. Winick, P. Wintersteiner, P. Espy, R. Garcia, R. G. Roble, and S. Solomon, "An overview and science results from the saber experiment on the timed satellite," *AGU Fall Meeting Abstracts*, pp. A1+, Dec. 2002.